IFASD 2015
International Forum on Aeroelasticity and Structural Dynamics
June 28 — July 02, 2015 ▲ Saint Petersburg, Russia

INTEGRATED FLEXIBLE DYNAMIC LOADS MODELS BASED ON AERODYNAMIC INFLUENCE COEFFICIENTS OF A 3D PANEL METHOD

Thiemo M. Kier[1], Mark J. Verveld[1], and Chris W. Burkett[2]

[1]DLR, German Aerospace Center
Institute of System Dynamics and Control
82234 Weßling, GERMANY
Thiemo.Kier@dlr.de
Mark.Verveld@dlr.de

[2]Flow Solutions Limited
Chipping Sodbury, UK
Chris@flowsol.co.uk

Keywords: integrated flexible flight dynamics model, manoeuvre loads analysis, 3D Panel Method, Aerodynamic Influence Coefficients

Abstract: The integration of loads analysis models using so called aerodynamic influence coefficients (AICs) is described. These AICs relate a change of normal velocity at panel control points to a change in panel pressure distribution, allowing to consider aeroelastic effects in a straight forward manner. The aerodynamic method employed for aeroelastic applications is typically the Vortex or Doublet Lattice Method, discretizing mean lifting surfaces. In this paper, the AICs are obtained by a 3D panel method, which significantly increases the geometric fidelity and accounts for previously unmodeled flight mechanical effects. These effects are verified by comparison with the Vortex Lattice Method and CFD results. Further, an interpolation scheme is required, since the AICs of 3D panel methods depend nonlinearly on the underlying flight state. The setup of a reduced order aerodynamic model for AICs (AIC-ROM), based on proper orthogonal decomposition is presented and results are assessed.

1 INTRODUCTION

For the certification of a new aircraft type, it has to be demonstrated that its structure can withstand the loads acting on it without damage. In order to design the structure accordingly, a so called loads envelope is computed. To determine this envelope, loads analysis models need to be simulated many times in the entire flight envelope at different air speeds, altitudes, mass cases and for different types of manoeuvres and gusts. Further, these models must account for the flexibility of the airframe and the resulting change in the distributed aerodynamic loading in order to determine the shear force, bending and torsion moment along the axes of the individual aircraft components. The number of required load cases can easily exceed the 100.000s.

Hence, loads analysis models need to be fast to simulate, but also sufficiently accurate, to cover this enormous amount of simulations. Clearly, for this type of application, the use of Computational Fluid Dynamics (CFD) coupled with Computational Structural Mechanics (CSM) is still too expensive, in spite of the impressive advances in recent computing

technology. Therefore, much faster aerodynamic methods are essential to handle the large number of simulations required for loads analysis. Typically, for these kind of aeroelastic applications, the aerodynamic methods are based on linear potential theory, which solve the (unsteady) Prandtl-Glauert equation. Traditionally, lifting surfaces methods such as the Vortex Lattice Method (VLM) [1], respectively its unsteady counterpart the Doublet Lattice Method (DLM) [2–4] are used. Since lifting surface methods discretize the mean surface of aerodynamic surfaces, merely the pressure difference between upper and lower surface is calculated. Further, in many "classical" implementations, like e.g the DLM available in the aeroelastic solutions of `Nastran`, there is no dependence on the onflow conditions. This is because the lifting force is calculated simply with a scalar multiplication of the circulation with the freestream velocity, instead of using a cross product of the circulation with the real onflow velocity. Hence, changes in lift direction and magnitude due to relative motion are not accounted for.

When the surface pressures are calculated by higher fidelity aerodynamic methods like Euler and RANS CFD solvers, the coupling with the structural dynamics and flight mechanics is usually done by co-simulation [5, 6]. The pressure loads and deflections are passed over between the aerodynamics code and the equation of motion of the flexible body, e.g. using predictor-corrector schemes. To reduce the simulation time, faster aerodynamic methods such as the previously mentioned panel methods can be used. However, still co-simulation strategies are often employed in this case [7, 8].

The approach in the present paper, is to obtain a linear relationship about a reference flight state between the normal velocities at the control points $\mathbf{w}_j$ and the perturbation surface pressures coefficients $\mathbf{c_p}$ of the individual panels, the so called Aerodynamic Influence Coefficient (AIC) matrix $\mathbf{Q}_{jj}$. The resulting AICs are fully populated, complex valued matrices of size n_{panels} by n_{panels}. They need to be setup only once in a preprocessing step and can then be reused in different loads analysis scenarios. In the AIC approach the pressures are obtained by a simple matrix multiplication, instead of recomputing the pressures at each time step for the changing flow conditions. This relationship allows to express the problem in a closed form, without having to resort to co-simulation. A fit of the unsteady transfer functions, the so called Rational Function Approximation (RFA) [9, 10], allows to express the problem as a system of nonlinear ordinary differential equations (ODE), which can be integrated in time using Runge-Kutta schemes.

In this paper, a 3D panel method is used to discretize the actual surface. The increased geometric fidelity enables to compute surface pressures of volumetric bodies and thick wings. The use of a 3D panel method also allows to account for effects, such as e.g. flight mechanical yaw-roll coupling and sideslip derivatives. In most lifting surface schemes, these effects are not present, due to early linearization and simplifying assumptions in their derivations. Similar to the well established vortex and doublet lattice method, the 3D Panel Method `NEWPAN` allows to output AIC matrices as a function of a harmonic excitation. Those AIC matrices allow for a straight forward replacement in loads and flutter analysis. This approach is then in line with classical aeroelasticity [11] using the VLM/DLM, but extending its fidelity and nonlinear aspects.

The present paper is concerned with using AICs from a 3D panel method for manoeuvre loads analysis. In [12] a first implementation of such an AIC approach was presented. In this paper, the focus lies on the validation of the previously neglected flight mechanical

effects and comparison with VLM results. Another important point is that, unlike in the VLM, the AIC matrices of the panel method are dependent on the steady flight state they are linearized about. Therefore, an interpolation scheme needs to be employed. The present paper introduces an approach based on proper orthogonal decomposition (POD) to set up a reduced order model (ROM). The difference to similar approaches where CFD results are interpolated [13] is that the current formulation operates on the AIC matrices instead of the pressures. The procedure of setting up this so called AIC-ROM and comparisons with direct steady calculations are presented. The advantages of the AIC-ROM over a direct interpolation of pressures are discussed.

To begin with, loads analysis model integration in general is discussed and the necessary equations are formulated. Next, gust and manoeuvre loads models and their specific requirements are assessed. Highlighted are the implications of a quasi-steady approximation for the aerodynamics in the light of manoeuvre loads analysis. The next section is concerned with the implications of using AICs from panel methods instead of lifting surface discretizations. The governing equations for the 3 D panel method and corresponding boundary conditions are presented. The aforementioned flight mechanical effects are examined and compared to CFD calculations. The implementation details of the aerodynamic model using the newly introduced AIC-ROM are outlined and compared to direct steady calculations. Finally, the results for a full aircraft configuration examined in [12], are assessed in the light of the improvements to the AIC approach presented in this paper.

2 LOADS ANALYSIS MODEL INTEGRATION AND SIMULATION

The model integration and simulation has been implemented in the loads analysis environment `VarLoads` [10, 14–19]. The following section describes the general principles regarding the integration aspects of the loads analysis model, i.e. the structural model, the equations of motion and the external forcing due to propulsion and the aerodynamics. The model equations in `VarLoads` are expressed in closed from, in contrast to co-simulation schemes in other simulation environments. I.e. similarly to classical aeroelasticity the gradient information of the AIC matrices is used. Furthermore, the equations are formulated as nonlinear system of ODEs to be amendable to time domain integration.

2.1 Structural Dynamics, Equations of Motion and Load Recovery

The starting point, when setting up the equations of motion for a loads analysis model for a flexible aircraft is an Finite Element Model (FEM). This FEM usually consists of 100.000s of degrees of freedom (DoFs). Static condensation can be used to reduce the problem size by several orders of magnitude. The method employed is known as the Guyan reduction [20], where condensation points ($g - set$) are placed along a loads reference axes. The mass distributions are prepared for the corresponding payload/fuel cases and connected to the $g - set$. Subsequently a modal analysis is carried out and only part of the modal basis is retained to further reduce the model size and computational cost.

The eigenvalues and eigenvectors define the generalized coordinates of the $h - set$. The zero eigenvalues represent the rigid body motion. The $h - set$ can be partitioned into six rigid body DoFs ($b - set$) and flexible part ($f - set$). The rigid body mode shapes $\mathbf{\Phi}_{gb}$ and

the retained modes of the eigenvector matrix $\mathbf{\Phi}_{gf}$ are used to generalized the equations of motion, which are given in the frequency domain by

$$\left\{-\omega^2 \begin{bmatrix} \mathbf{M}_{bb} & \mathbf{0} \\ \mathbf{0} & \mathbf{M}_{ff} \end{bmatrix} + \mathrm{j}\,\omega \begin{bmatrix} \mathbf{0} & \mathbf{0} \\ \mathbf{0} & \mathbf{B}_{ff} \end{bmatrix} + \begin{bmatrix} \mathbf{0} & \mathbf{0} \\ \mathbf{0} & \mathbf{K}_{ff} \end{bmatrix}\right\} \begin{bmatrix} \mathbf{u}_b \\ \mathbf{u}_f \end{bmatrix} = \begin{bmatrix} \mathbf{\Phi}_{gb}^{\mathrm{T}} \\ \mathbf{\Phi}_{gf}^{\mathrm{T}} \end{bmatrix} \mathbf{P}_g^{ext}(\omega). \tag{1}$$

Note that the rigid body $b-set$ DoFs in (1) are defined in a earth fixed coordinate frame.

A suitable set of equations of motion to account for large rigid body motions and linear flexibility is derived in the references [21–24]. The nonlinear equations of motion describe the movement relative to a "mean axes" body reference frame. Equations of motion for an unrestrained flexible aircraft accounting for large rigid body motions are given by

$$\begin{aligned} \begin{bmatrix} \mathbf{m}_b \left(\dot{\mathbf{V}}_b + \mathbf{\Omega}_b \times \mathbf{V}_b - \mathbf{T}_{bE}\, \mathbf{g}_E\right) \\ \mathbf{J}_b \dot{\mathbf{\Omega}}_b + \mathbf{\Omega}_b \times (\mathbf{J}_b \mathbf{\Omega}_b) \end{bmatrix} &= \mathbf{\Phi}_{gb}^{\mathrm{T}} \mathbf{P}_g^{\mathrm{ext}}(t) \\ \mathbf{M}_{ff}\ddot{\mathbf{u}}_f + \mathbf{B}_{ff}\dot{\mathbf{u}}_f + \mathbf{K}_{ff}\mathbf{u}_f &= \mathbf{\Phi}_{gf}^{\mathrm{T}} \mathbf{P}_g^{\mathrm{ext}}(t), \end{aligned} \tag{2}$$

where $\mathbf{\Phi}_{gb}$ is the rigid body modal matrix about the center of gravity and in directions as customary in flight mechanics, i.e x-forward, z-down. $\mathbf{V}_b$ and $\mathbf{\Omega}_b$ are the velocity, respectively angular velocity vectors in the body frame of reference. The matrix $\mathbf{T}_{bE}$ transforms the gravitational vector from an earth fixed (E) to the body fixed coordinate frame (b) as a function of Euler angles.

In order to recover the nodal loads $\mathbf{P}_g$ for a subsequent sizing of the structure, the force summation method (FSM) [11] is employed. Thus, subtraction of the inertial loads $\mathbf{P}_g^{\mathrm{iner}}$ from the external loads, yields

$$\mathbf{P}_g = \mathbf{P}_g^{\mathrm{ext}} - \underbrace{\mathbf{M}_{gg} \left\{\mathbf{\Phi}_{gb}\, \ddot{\mathbf{u}}_b \quad + \quad \mathbf{\Phi}_{gf}\, \ddot{\mathbf{u}}_f\right\}}_{\mathbf{P}_g^{\mathrm{iner}}} \tag{3}$$

In the case of the nonlinear equations of motion (2), the rigid body acceleration is given as

$$\ddot{\mathbf{u}}_b = \begin{bmatrix} \dot{\mathbf{V}}_b + \mathbf{\Omega} \times \mathbf{V}_b - \mathbf{T}_{bE}\, \mathbf{g}_E \\ \dot{\mathbf{\Omega}}_b + \mathbf{J}_b^{-1} \left(\mathbf{\Omega}_b \times (\mathbf{J}_b \mathbf{\Omega}_b)\right) \end{bmatrix}. \tag{4}$$

The FSM requires the external forces to be available on the structural grid. This allows to accounts for the static part directly on the physical grid, and therefore has a good convergence behavior. Then cut loads can be computed by integrating the nodal loads along the loads reference axes of each aircraft component. The envelope of the cut loads is used as sorting criteria to obtain the critical load cases used for the structural sizing.

2.2 External Forces: Aerodynamics and Propulsion

With the equations of motion defined, the external forces have to be determined. One source of these external forces is the propulsion. The propulsion forces are simply modeled as concentrated forces at the engine locations, accounting for thrust as well as gyroscopic loads.

The other major contribution to the excitation forces $\mathbf{P}_g^{\mathrm{ext}}$ stem from the aerodynamics. In aeroelastic applications the aerodynamic pressures are determined by using a linear

relationship between the normalwash at the control point to the panel pressure, i.e. a change of the flow, normal to the panel surface at control point results in a change in pressure distribution. This allows to easily account for flexible deformation, which are simply treated as change in the normalwash vector $\mathbf{w}_j$. The pressure coefficients are computed by

$$\Delta \mathbf{c_p}_j = \mathbf{Q}_{jj}\ \mathbf{w}_j, \tag{5}$$

where $\mathbf{Q}_{jj}$ is the so called AIC matrix. Traditionally, the Vortex Lattice and the Doublet Lattice Methods are used to obtain these AIC matrices. The Doublet Lattice Method provides the complex valued AIC matrix as function of reduced frequency $k = \frac{c_{ref}/2}{U_\infty}\omega$, which describe the unsteady aerodynamic transfer functions. In frequency domain calculations, cf. equation (1) the complex AICs can be used directly. For time domain simulations, a Rational Function Approximation (RFA) [9, 10], is required to transform the AICs to the Laplace domain. The rational functions can then be cast in form of a system of linear ordinary differential equation amendable to time integration.

The load transformation to panel reference point is done by integrating the pressures, which is mostly a simple multiplication with the aerodynamic box area. In some classical aerodynamic panel methods additional moments occur due to an offset between control point and pressure application point, cf. [25]. These are accounted for by introducing rotational degrees of freedom in the aerodynamic panel ($k-set$) and the respective moment arms into the integration matrix $\mathbf{S}_{kj}$. Multiplication with the dynamic pressure yields the aerodynamic forces.

$$\mathbf{P}_k^{\text{aero}} = q_\infty\ \mathbf{S}_{kj}\ \mathbf{c_p}_j \tag{6}$$

Next, the boundary condition for the normalwash has to be considered:

$$\mathbf{w}_j(k) = \left(\mathbf{D^x}_{jk} + \frac{\mathrm{d}}{\mathrm{d}t}\left(\frac{c_{ref}/2}{U_\infty}\right)\cdot\ \mathbf{D^t}_{jk}\right)\ \mathbf{u}_k(t), \tag{7}$$

where the matrix $\mathbf{D^x}_{jk}$ accounts for a change in downwash due to a change of the normal vector with respect to the free stream direction and the matrix $\mathbf{D^t}_{jk}$ for additional downwash due to movement of the boundary in direction of the panel normal. The factor $\frac{c_{ref}/2}{U_\infty}$ in equation (7) is needed due to the conversion from reduced to natural frequency. The vector $\mathbf{u}_k(t)$ represents the motion of the aerodynamic reference points.

When the nonlinear equations of motion (2) are used, special attention to the boundary condition is required. The vectors $\mathbf{V}_b$ and $\mathbf{\Omega}_b$ are defined in a body carried frame of reference. Hence, the steady deflection of rigid body modes does not induce aerodynamic loads. Therefore, the differentiation matrix $\mathbf{D^x}$ needs to be canceled for the rigid body modes. Otherwise, this would imply that the orientation (Euler angles) of the aircraft would directly result in additional aerodynamic forces. The cancelation of the differentiation matrix is equivalent to a coordinate transformation from an earth fixed to a body fixed coordinate system.

Finally, the aerodynamic loads have to be mapped to the structural degrees of freedom. The matrix connecting the displacements of the structural grid ($g-set$) to the aerodynamic grid ($k-set$) is called spline matrix $\mathbf{T}_{kg}$.

$$\mathbf{u}_k = \mathbf{T}_{kg}\mathbf{u}_g \tag{8}$$

This mapping is achieved, e.g. by employing radial basis functions, such as the commonly used Infinite Plate Spline (IPS) [26], or by using beam splines [27]. The physical interpretation is that the structure behaves plate or beam like and that the respective degrees of freedom sets $k-set$ and $g-set$ lie on the same structure described by the spline basis functions. The aerodynamic loads can be mapped back onto the structure with the transpose of the spline matrix, based on the principal of virtual work.

$$\mathbf{P}_g^{\text{aero}} = \mathbf{T}_{kg}^{\text{T}} \mathbf{P}_k^{\text{aero}} \tag{9}$$

Similarly, the modal matrix $\mathbf{\Phi}_{gf}$, and its transpose connect the flexible part of the equations of motion (1) and (2) to the aerodynamic model.

2.3 Manoeuvre and Gust Loads Simulation

Flight loads analysis models can be classified into two categories, manoeuvre loads and gust loads models. Models for manoeuvre loads analysis are based on nonlinear rigid body equations of motion to account for large amplitude responses as a result from prescribed pilot inputs. This necessitates an aerodynamic database, covering the nonlinearities in the flight regime of interest. Models for gust loads analysis on the other hand, only consider small perturbations around a trimmed flight state. In this case, both structural dynamics as well as unsteady aerodynamic effects are important. The unsteady aerodynamic increments are usually considered to be linear.

In [10] an approach to unify these models has been presented, where on top of the manoeuvre analysis aspects, the unsteady aerodynamics are modeled as an additional effect by means of a RFA of the frequency domain transfer function. This unified modeling approach allowed the separation of the quasi-steady from the unsteady aerodynamic effects. Of course the gust can also be calculated using frequency domain approaches which result in a load increment, which has to be superimposed with the trim result of the aircraft in horizontal flight. The gust and turbulence required for the loads analysis are specified in paragraph CS 25.341 of the airworthiness requirements CS 25 subpart C [28].

Compared to a gust load case, the change of normal-wash at the control points for a manoeuvring aircraft can be considered slow, i.e. the spectral content of the excitation is limited to low frequencies. In this case the quasi steady assumption holds, i.e. that there is neither a change in magnitude and nor a phase shift in the aerodynamic transfer functions over the low frequency range. E.g. in unsteady incompressible 2D airfoil aerodynamics this implies that the Theodorsen function [29] is constant over the reduced frequency range with its value for $k = 0$, i.e. a value of one. Equivalently, for the aircraft geometry this means that the AIC matrix at a reduced frequency of zero can be used to compute the pressures for all low excitation frequencies.

This is in line with the general approach for flight mechanical simulations. However, one notable unsteady addition is commonly incorporated: the lag in downwash from the wing to the empennage is modeled by use of the $\dot{\alpha}$-derivatives and air speed dependent time delays. The major difference between flight mechanical models and manoeuvre loads models is the necessity in loads analysis to account for distributed aerodynamic forces over the entire airframe, instead of just computing the aircraft total force and moment coefficients to feed the rigid body equations of motion. This results in a significant increase

of the modeling effort, which is usually accounted for by sacrificing some level of detail concerning the nonlinearities in the aerodynamic database.

The manoeuvres that have to be simulated for loads analysis are specified in the CS 25 subpart C [28]. These so called design manoeuvres include, e.g. symmetrical pull up and push over manoeuvres (CS 25.331), accelerated and steady roll manoeuvres (CS 25.349), one sided engine failures (CS 25.367), or yawing manoeuvres (CS 25.351). Some of these can be covered by trim calculations as e.g. the symmetrical 2.5g pull-up, others need to be simulated in time, particularly when interaction with flight control laws or pilot response needs to be considered.

3 AERODYNAMIC INFLUENCE COEFFICIENTS USING A 3D PANEL METHOD

Instead of employing the mean lifting surface discretization of the Vortex, respectively Doublet Lattice Method, now a three dimensional panel method is used to model the flow about the actual surface with quadrilateral or triangular panels. The panel method `NEWPAN` [30] from Flow Solutions Limited calculates the steady mean flow pressures, as well as the complex perturbation pressures about this steady state, due to harmonic excitation. `NEWPAN` is also able to output complex AIC matrices, which allow for a direct integration in the previously described model integration scheme.

3.1 Aerodynamic Governing Equations

The derivation of the governing flow equations solved by the panel method, proceeds in two stages. First, the steady flow about the mean surface is associated with the steady velocity potential Φ_S. The governing equation is given by the steady Prandtl-Glauert equation:

$$\left(1 - M_\infty^2\right) \frac{\partial^2 \Phi_S}{\partial x^2} + \frac{\partial^2 \Phi_S}{\partial y^2} + \frac{\partial^2 \Phi_S}{\partial z^2} = 0 \tag{10}$$

Using a Göthert Type 2 transformation [31], the problem can be reduced to a Laplace type equation $\nabla^2 \Phi_S = 0$.

This steady solution about a, possibly deformed reference shape, defines the flight state about which an unsteady linearization is performed. The unsteady solution is then found by solving the linearized frequency domain variant of the unsteady Prandtl-Glauert equation

$$\left(1 - M_\infty^2\right) \frac{\partial^2 \Phi_U}{\partial x^2} + \frac{\partial^2 \Phi_U}{\partial y^2} + \frac{\partial^2 \Phi_U}{\partial z^2} - 2\mathrm{j}\omega \frac{M_\infty}{a_\infty} \frac{\partial \Phi_U}{\partial x} - \left(\frac{\omega^2}{a_\infty^2}\right) \Phi_U = 0, \tag{11}$$

where the unsteady potential is given as $\mathrm{e}^{\mathrm{j}\omega t}\, \Phi_U(x, y, z)$. This equation can be converted to a Helmholtz type equation

$$\nabla^2 \Phi_U + \kappa^2 \Phi_U = 0, \quad \text{with} \quad \kappa = k \frac{M_\infty}{1 - M_\infty^2}, \tag{12}$$

to determine the solution, where κ is a frequency parameter depending on the reduced frequency and Mach number. The total velocity potential is then $\Phi(x, y, z, \omega) = \Phi_S(x, y, z) + \mathrm{e}^{\mathrm{j}\omega t}\, \Phi_U(x, y, z)$, from which the complex unsteady pressure is calculated via a linearized version of the unsteady Bernoulli equation.

To obtain the steady mean flow from `NEWPAN`, the flight state is specified by the Mach number M_∞, the angle of attack α and sideslip β, as well as the normalized roll, pitch and yaw rates (p_n, q_n and r_n). Further the control surfaces can be deflected by a rotation of the corresponding normal vectors about a given hingeline.

The unsteady flow is then calculated as a function of reduced frequency about this steady flight state in a small perturbation sense. By default the complex pressures for the rigid body and control surface modes are computed. Additionally, structural modes can be defined as displacement vectors of the nodes of the surface panel mesh. For the unsteady flow calculation also the AIC matrices can be obtained at specified reduced frequencies. These can then be used for external computation of the pressures, e.g. for gust load or flutter calculations. The AIC matrix for $k = 0$ is real valued and can be used in manoeuvre loads analyses, adhering to a quasi-steady approximation.

Some differences and direct ramifications of using 3D panel method versus the commonly used DLM should be noted. The DLM also solves the unsteady Prandtl-Glauert equation (11), however Φ_U represents the acceleration (or pressure) potential rather than the velocity potential. Otherwise, the governing equation are formally equivalent, i.e. the same type of elementary solutions, such as doublets and sources are valid. The DLM directly yields the pressure difference, hence no pressure recovery via the Bernoulli equation is required. However, an integration has to be performed to obtain the velocities, which are required to satisfy the flow tangency condition at the control point. Another direct result from using the acceleration potential is the absence of a modeled wake, since there is no pressure jump across the wake. The DLM solution implicitly accounts for a flat wake in free stream direction.

Further, when thick bodies are modeled in potential flow, additional pressure contributions arise. These are not associated with the normalwash, but with tangential flow at the panels. Therefore, the 3D Panel Method, requires the additional motion induced terms $\mathbf{DP^x}_{jk}$ and $\mathbf{DP^t}_{jk}$. It should be noted that these terms are dependent on the onflow direction, i.e. they are associated with the flight state, about which the AIC was linearized.

The perturbation pressures $\delta\,\mathbf{c_p}$ about the reference state are given as

$$\delta\,\mathbf{c_p}_j(k) = \left[\mathbf{Q}_{jj}\ \left(\mathbf{D^x}_{jk} + \mathrm{j}k\cdot\ \mathbf{D^t}_{jk}\right)\ + \left(\mathbf{DP^x}_{jk} + \mathrm{j}k\cdot\ \mathbf{DP^t}_{jk}\right)\right]\ \mathbf{u}_k(k). \tag{13}$$

Hence, in the DLM any coupling between the steady and unsteady flow is lost, which is accounted for by the 3D panel method intrinsically.

3.2 Generalized Aerodynamic Forces

During time integration with a higher order Runge-Kutta schemes, the model is evaluated many times per time step. Therefore, to shorten the simulation times, merely the generalized aerodynamic forces due to the inputs that are driving the equations of motion (2) are computed. The required inputs that induce aerodynamic loads are given by the rigid body velocities $\mathbf{V}_b$ and rates $\mathbf{\Omega}_b$ (abbreviated by $\dot{\mathbf{u}}_b$), the control surface deflections denoted by $\mathbf{u}_{x2}$, the flexible modal displacements $\mathbf{u}_f$ and the corresponding flexible modal velocities $\dot{\mathbf{u}}_f$. Instead of directly using the rigid body velocities $\dot{\mathbf{u}}_b$ defined about the center of gravity, the typical quantities about an aerodynamic reference point, namely α, β and roll, pitch and yaw rates (p_n, q_n, r_n) normalized by free stream velocity and reference

length $\frac{U_\infty}{c_{ref}}$ are computed. These quantities are assembled in a rigid body aerodynamic state vector and denoted $\mathbf{u}_{x1}$.

The gradient information of the AIC matrices is expressed in generalized influence coefficient matrices at each linearization point. Required are the effects due to rigid body aerodynamic states,

$$\mathbf{Q}_{hx1} = \mathbf{\Phi}_{gh}^{\mathrm{T}}\ \mathbf{T}_{kg}^{\mathrm{T}}\ \mathbf{S}_{kj}\ \left[\mathbf{Q}_{jj}\mathbf{D^t}_{jk} + \mathbf{DP^t}_{jk}\right]\ \mathbf{\Phi}_{kx1} \tag{14}$$

due to control surface deflections,

$$\mathbf{Q}_{hx2} = \mathbf{\Phi}_{gh}^{\mathrm{T}}\ \mathbf{T}_{kg}^{\mathrm{T}}\ \mathbf{S}_{kj}\ \left[\mathbf{Q}_{jj}\mathbf{D^x}_{jk} + \mathbf{DP^x}_{jk}\right]\ \mathbf{\Phi}_{kx2} \tag{15}$$

due to modal displacements,

$$\mathbf{Q}_{hf} = \mathbf{\Phi}_{gh}^{\mathrm{T}}\ \mathbf{T}_{kg}^{\mathrm{T}}\ \mathbf{S}_{kj}\ \left[\mathbf{Q}_{jj}\mathbf{D^x}_{jk} + \mathbf{DP^x}_{jk}\right]\ \mathbf{T}_{kg}\mathbf{\Phi}_{gf} \tag{16}$$

and due to modal velocities

$$\mathbf{DQ}_{hf} = \mathbf{\Phi}_{gh}^{\mathrm{T}}\ \mathbf{T}_{kg}^{\mathrm{T}}\ \mathbf{S}_{kj}\ \left[\mathbf{Q}_{jj}\mathbf{D^t}_{jk} + \mathbf{DP^t}_{jk}\right]\ \mathbf{T}_{kg}\mathbf{\Phi}_{gf}. \tag{17}$$

These individual contributions can be concatenated to the generalized aerodynamic force matrix $\mathbf{Q}_{hx}$, such that the generalized aerodynamic forces are:

$$\mathbf{P}_h^{\mathrm{aero}} = q_\infty \left[\mathbf{Q}_{hx1}\cdot\mathbf{u}_{x1} + \mathbf{Q}_{hx2}\cdot\mathbf{u}_{x2} + \mathbf{Q}_{hf}\cdot\mathbf{u}_f + \mathbf{DQ}_{hf}\cdot\frac{U_\infty}{(c_{ref}/2)}\dot{\mathbf{u}}_f + \mathbf{Q}_{h0}\right] = q_\infty\left[\mathbf{Q}_{hx}\cdot\mathbf{u}_x + \mathbf{Q}_{h0}\right] \tag{18}$$

The term $\mathbf{Q}_{h0}$ is the intercept of the generalized aerodynamic forces of the given flight point. The steady pressure coefficients at the linearization flight state $\mathbf{u}_{x_{\mathrm{lin}}}$ are given by $\mathbf{c}_{p_{\mathrm{lin}}}$. The intercept values are then calculated by

$$\mathbf{Q}_{h0} = \mathbf{\Phi}_{gh}^{\mathrm{T}}\ \mathbf{T}_{kg}^{\mathrm{T}}\ \mathbf{S}_{kj}\ \left(\mathbf{c}_{p_{\mathrm{lin}}} - \mathbf{Q}_{hx}\cdot\mathbf{u}_{x_{\mathrm{lin}}}\right). \tag{19}$$

The matrices (14)-(19) can be set up in a model initialization phase. This way, the sizes of the matrices are kept as small as possible, allowing for significantly shortened simulation times. It should be noted that those matrix sizes are independent of the number of panels of the underlying panel model. Hence, the additional computational cost for larger aerodynamic models is confined to the preprocessing phase. Pressures and physical structural forces, required for the loads recovery are then calculated in a postprocessing step based on the trajectory generated by the simulation.

3.3 Previously Unaccounted Flight Mechanical Effects

One of the major advantages of panel methods over the "classical" Vortex Lattice Method, is the ability to account for additional flight mechanical effects, such as rolling moment due to sideslip $C_{\mathcal{L}_\beta}$, rolling moment due to yaw rate $C_{\mathcal{L}_r}$, and yawing moment due to roll rate C_{N_p}. These effects are also essential in calculating flutter boundaries for T-tailed aircraft. The missing terms can also be accounted for by augmenting the DLM results with values from strip theory [32]. Good results were also obtained by using a more general formulation, such as the Unsteady Vortex Lattice Method (UVLM) [33], which, however, is limited to the incompressible flow regime. Also, the methods classically used in aeroelastics can be improved. Enhancements to the VLM in order to account for flight

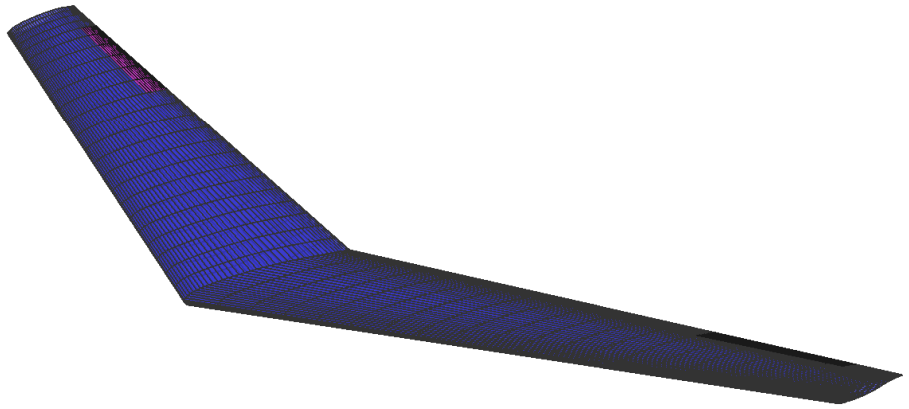

Figure 1: Panel mesh of LANN wing.

mechanical effects and induced drag were proposed in reference [10]. Further, the DLM was extended comprehensively for T-tails flutter calculations in references [34] and [35]. The 3D panel methods inherently accounts for all of the previously mentioned effects in a coherent way and the ability to provide frequency dependent AIC-matrices makes it suitable for a direct replacement in most aeroelastic procedures.

For demonstration of the effects in question, the LANN wing [36] was chosen as test case. The flight state was set at $Ma = 0.65$ and $\alpha = 0°$. A set of available CFD calculations solving the inviscid Euler equations was used to further validate the 3D panel method. The gradient information due to the different excitations was obtained by finite differences. The panel model depicted in figure 1 has 3588 panels and includes control surfaces. The comparisons include the gradients obtained from the CFD calculations, the AIC matrices of the VLM, the `Newpan` AIC matrices, and values from a finite difference calculation of two steady `Newpan` calculations. The axis system used for all the computations is x-backward, y-right, z-up, with the origin chosen at the wing apex. The results are always given in this body fixed reference frame, for simplicity the forces in z and x are referred to as lift and drag.

Figure 2 shows the lift and moment gradients with respect to α. The perturbation step size was 1° for the finite difference calculation. The result of the potential flow methods correlate well, the lift gradient for the CFD calculation is somewhat larger. The VLM underestimates the gradients for both lift and moment, while the 3D panel method seems to capture the moment distribution quite well. It should be noted that this amounts to a small difference in the position of the neutral point. Further, it should be pointed out that no deeper convergence checks were carried out for any of the CFD calculations. Generally, the results match well and the flight mechanical effects of interest can now be examined.

The first effect to be examined is the rolling moment due to sideslip $C_{\mathcal{L}_\beta}$. Again the perturbation step was 1° for the sideslip angle β. The panel method results show excellent correlation with the CFD results for all of the gradient distributions in drag, lift and moment, depicted in figure 3. As expected the "classical" VLM is not able to capture any of these effects associated with beta. Integration of the lift over the span, yields the desired rolling moment coefficient $C_{\mathcal{L}_\beta}$. To illustrate the importance of the additional terms in equation (13), the distributions without those terms are included as well.

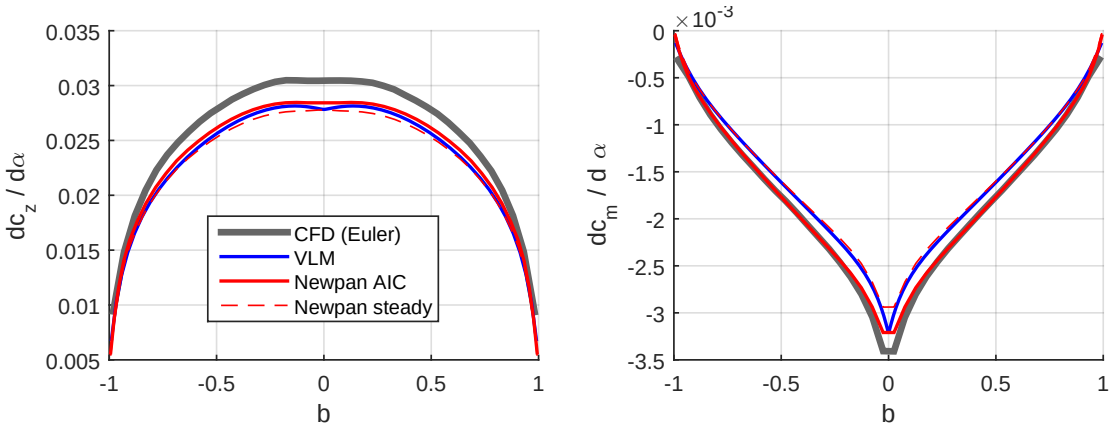

Figure 2: Lift and moment gradient distribution due α.

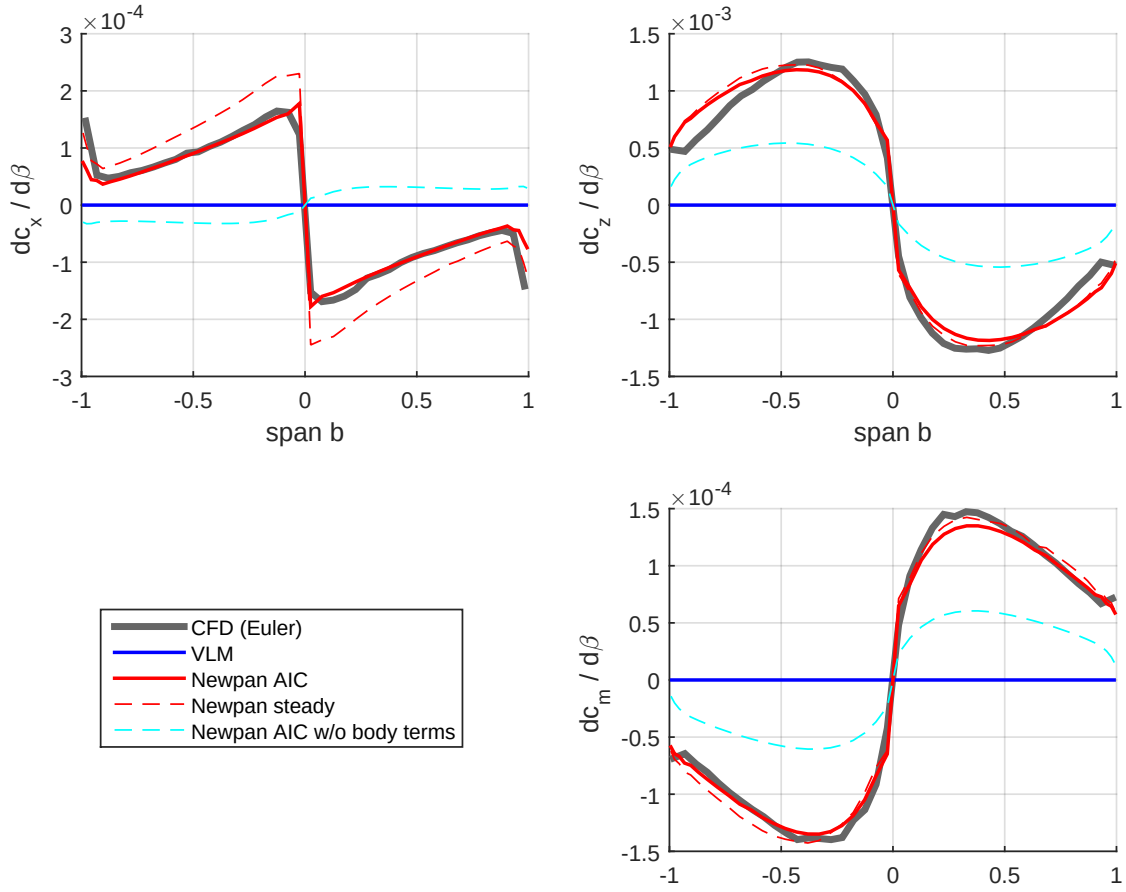

Figure 3: Drag, lift, and moment gradient distribution due β.

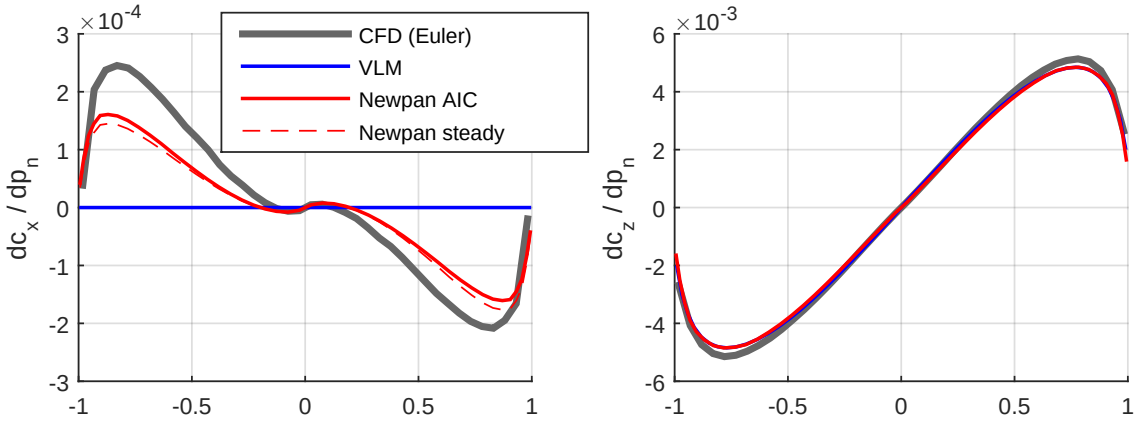

Figure 4: Drag and lift gradient distribution due roll rate p_n.

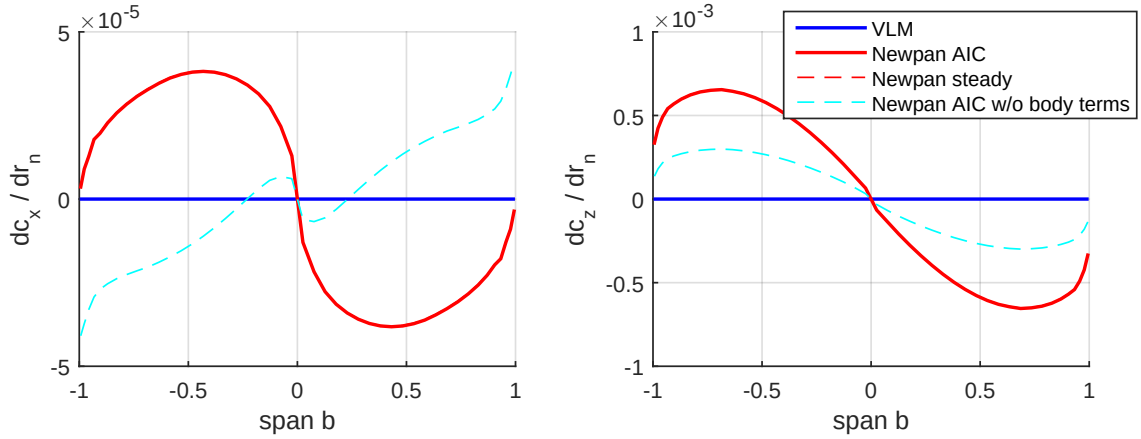

Figure 5: Drag and lift gradient distribution due yaw rate r_n.

Another effect is the yawing moment due to roll rate C_{N_p}. Lift and Drag distributions are shown in figure 4. The lift distribution is well captured by both potential flow methods. The forces in x-direction are induced by a change of angle of attack along the wing span due to the roll rate. Since the "classical" VLM does not capture the direction of lift, those forces are zero. In contrast, the panel method shows an distribution of the forces in x, however, somewhat lower when compared to the CFD results. The value for the yawing moment coefficient C_{N_p} is obtained by integration of the distribution over the span.

Unfortunately, there were no conclusive CFD results available for the yaw rate case . The distributions in figure 5 are therefore only useful for a qualitative statement. It should also be noted that for the chosen reference flight state at $\alpha = 0°$, the static loading is very low, since the wing is only slightly cambered. The lift distribution for the panel method shows an increase in lift for the advancing wing and a decrease for the receding, which yields the expected rolling moment due to yaw rate $C_{\mathcal{L}_r}$. Similarly to the distribution due to sideslip β the additional terms in (13) are of major importance.

It can be concluded that the panel method `Newpan` is able to account for previously neglected flight mechanical effects, which significantly increases the fidelity and correctness of the simulation. In particular flight mechanical modes such as the dutch roll are not captured correctly if these derivatives are neglected. This is also of interest when lateral gusts exciting the dutch roll mode are considered. Usually there is a gap between the flight mechanical simulation capturing the lower frequency flight mechanical modes well and the

gust load model tailored to account for structural dynamics and unsteady aerodynamics. Using AICs from a 3D panel method can ensure consistency between both model types.

Those effects are also major contributors in the T-tail flutter problem and are intrinsically included in the 3D panel method formulation.

3.4 Generation of an AIC based Reduced Order Model

The AIC matrices of the 3D panel method depend nonlinearly on the flight state, unlike the VLM, where there is no such dependency. Therefore, the AICs have to computed for range of parameters in the flight envelope and an appropriate scheme to interpolate between them is required.

The proper orthogonal decomposition (POD), also known as principle components analysis or Karhunen Loéve expansion, is a commonly used order reduction method with a broad range of applications, fluid dynamic problems being among them [13]. In general, it is a linear method which establishes an optimal basis, or modal decomposition, of an ensemble of continuous or discrete functions. The goals of applying the POD here are twofold: the POD enables to exploit similarity within a cluster of panel method results in a subspace of the flight envelope, thereby preserving the essential information by means of a only a few basis vectors. More importantly, paired with interpolation, any desired flight condition within this subspace can be approximated, producing a reduced order model (ROM). This ROM can then be evaluated efficiently in transient manoeuvre loads simulations.

The novelty in the present approach is that the POD is applied to AIC matrices rather than pressures, i.e. it is not necessary to build up a ROM for all parameters required in the simulation, but only for those parameters where the major nonlinearities occur, e.g. α and β. All other parameters like flexibility, rotation rates, or control surface deflections can be deduced from the AIC matrix gradient information in a linearized fashion about the nonlinearly interpolated flight state.

This AIC-ROM consists of two distinct PODs, one for the AIC matrices $\mathbf{Q}_{hx}$ and one for the pressure intercepts $\mathbf{Q}_{h0}$ of equation (18). The latter is similar to the classical pressure ROMs [13], with the exception that the values at the axes intercepts of the flight state are used, rather than the values at the actual flight point, cf. equation (19). For the first POD, the individual AIC matrices are reshaped as column vectors, to setup the snapshot matrix. Considerations of energy preservation then lead to the number of retained eigenvectors used for the AIC-ROM and hence to the amount of data compression. In the present work, the interpolation for the nonlinear flight state variables is based on the thin plate spline (TPS); other schemes are of course also possible. More details on that approach will be published soon.

Once more, the LANN wing was chosen to compare the results AIC-ROM with direct `Newpan` computations. First, a set of flight states were chosen to set up the AIC-ROM. The Mach number was fixed at $Ma = 0.65$. `USNewpan` was then used to compute the quasi-steady AIC matrices for $k = 0$ about four different flight states, i.e. for a range of angles of attack $\alpha = 0°, 5°, 10°$ with $\beta = 0°$ and a side slip case at $\alpha = 0°$ with $\beta = 10°$. The POD for the AIC matrices was setup and all eigenvectors were retained. Then a

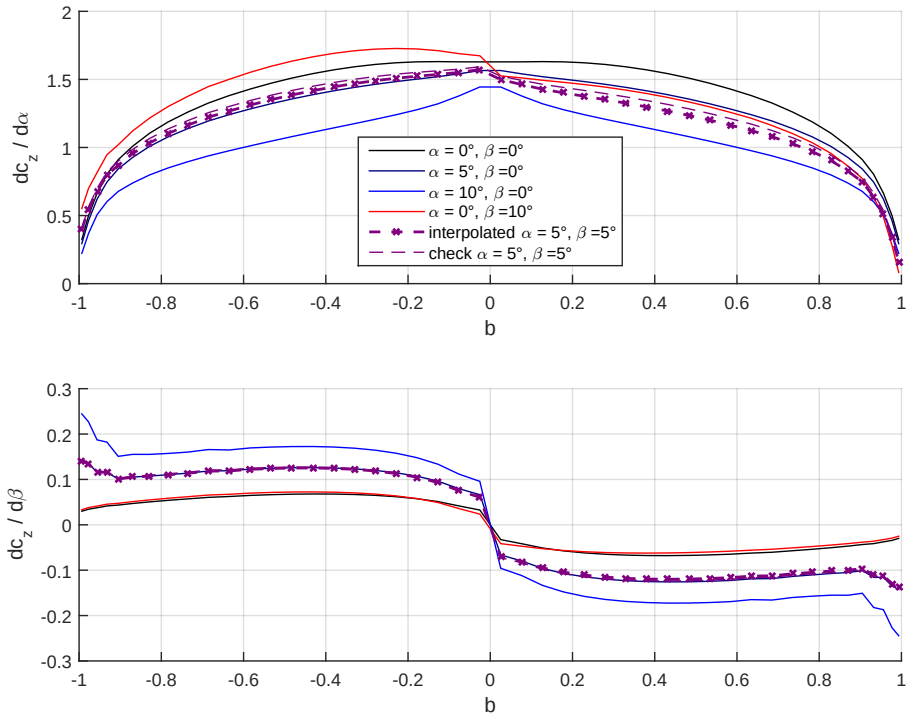

Figure 6: Lift gradient distributions due α and β.

matrix $\mathbf{Q}_{hx}(\alpha, \beta)$ was interpolated at $\alpha = 5°$ and $\beta = 5°$, using the previously described procedure. The interpolated results are then compared to an AIC matrix directly calculated by `USNewpan`. The comparison of lift gradients due to α and β are depicted in figure 6. For reference, the gradient distributions for the input of the POD are also included. The dependency of the AICs on the flight state is clearly visible, emphasizing the requirement for an interpolation. The result of the interpolation and the computed check case correlate very well.

The ROM of the gradient information yields very good results, however, for manoeuvre simulations, the total lift and moment distributions drive the equations of motion. Therefore, the AIC-ROM including the intercept values $\mathbf{Q}_{h0}$ is evaluated at a random flight state and compared to the results of a steady panel method run. The flight state selected for this case is $\alpha = 8°$, $\beta = 1°$, $p_n = 1.5°/s$, $\delta_{\text{ail}} = 10°$. In figure 7 the evaluation of the AIC-ROM is compared to a direct steady `Newpan` calculation. Further the flight state was also computed using a single AIC matrix linearized about $\alpha = 0°$, $\beta = 0°$. The agreement of the AIC-ROM evaluation and the steady reference calculation is excellent. Also the necessity to use interpolated AICs becomes evident when comparing the results to the distributions evaluated with a single AIC far away from the linearization point.

In this example, the advantages of the AIC-ROM become apparent. The ROM was setup only with AIC matrices related to the (nonlinear) flight parameters α and β. The other parameters roll rate p_n and aileron deflection δ_{ail} are inferred from the linear gradient information of the AIC matrices. This is particularly useful for aeroelastic simulations, where the structural flexibility can be treated in the same way. If the ROM was set up using directly the pressures instead of the AICs, the parameter space for aeroelastic simulation would be vastly increased.

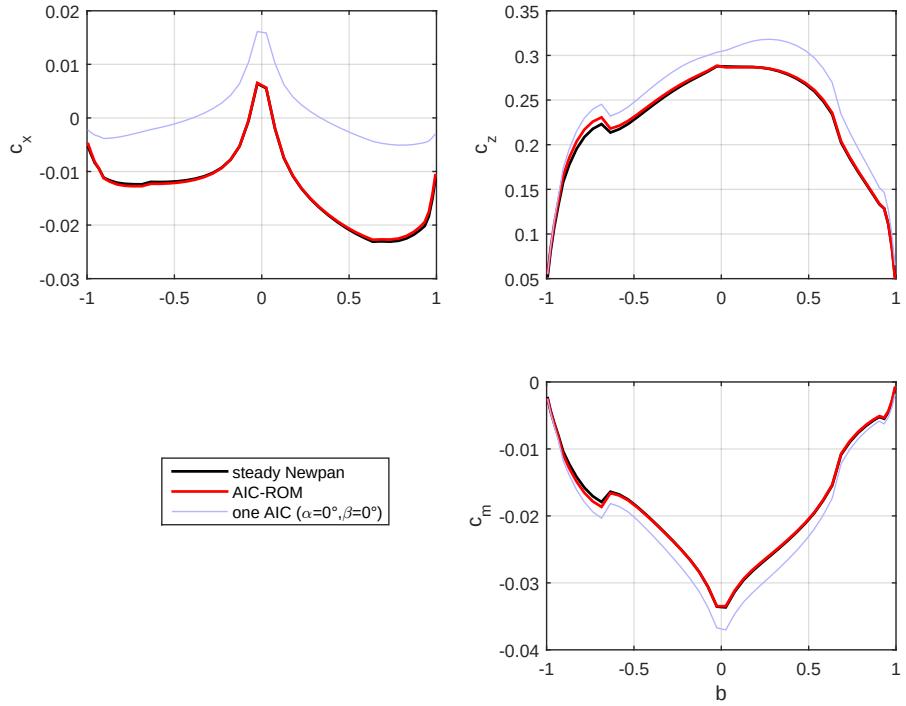

Figure 7: Drag, lift, and moment distributions at flight state $\alpha = 8°$, $\beta = 1°$, $p_n = 1.5°/s$, $\delta_{\text{ail}} = 10°$. Comparison of a reference calculation, the AIC-ROM, and using a single AIC matrix at linearization point $\alpha = 0°$, $\beta = 0°$

3.5 Results for a Full Aircraft Configuration

In [12] an aerodynamic panel model of a full aircraft configuration was used for simulation of two loads scenarios. A trim solution of a 2.5 g symmetrical pull-up and a transient roll manoeuvre. The panel model, depicted in figure 8, consists of ca. 15000 panels with eight individual control surfaces allocated to three pilot inputs for pitch, roll and yaw commands. The structural model is described by 90 flexible and 6 rigid body modes. The AIC matrices, set up in the preprocessing (equation (18)), have 186 inputs ($x - set$) (5 rigid body aerodynamic states, 3 pilot inputs, 90 modal displacements and 90 modal velocities) and 96 outputs ($h - set$) (6 rigid body forces and moments and 90 flexible generalized aerodynamic forces). These simulations of [12] were still lacking some of the features described in the present paper. Namely the additional body terms of equation (13) were missing, which, as shown in section 3.3, have a significant impact on the solution for the effects due to sideslip and yaw rate. Further, only a simple linear interpolation of merely two AIC matrices obtained at $\alpha = 0°$ and $\alpha = 10°$ was employed. The results using the described AIC-ROM approach are expected to vastly improve the accuracy of the simulation results. It was considered worthwhile to show those results again in the current context, since the AIC approach is particularly wellsuited for the flexible, aeroelastic effects excited in those scenarios.

A symmetrical pull-up manoeuvre with $N_z = 2.5$g, as specified in paragraph 25.331 of the CS 25 [28], was trimmed. The resulting angle of attack was at $\alpha = 11.5°$ and hence very close to the flight states, where one of the AICs was obtained. Hence, no detrimental effects due to the crude interpolation scheme are to be expected. The results of the lift distribution of the flexible aircraft are shown in figure 9. The AIC approach (red circles) is compared to the Panel Method (black crosses). The correlation between the results is

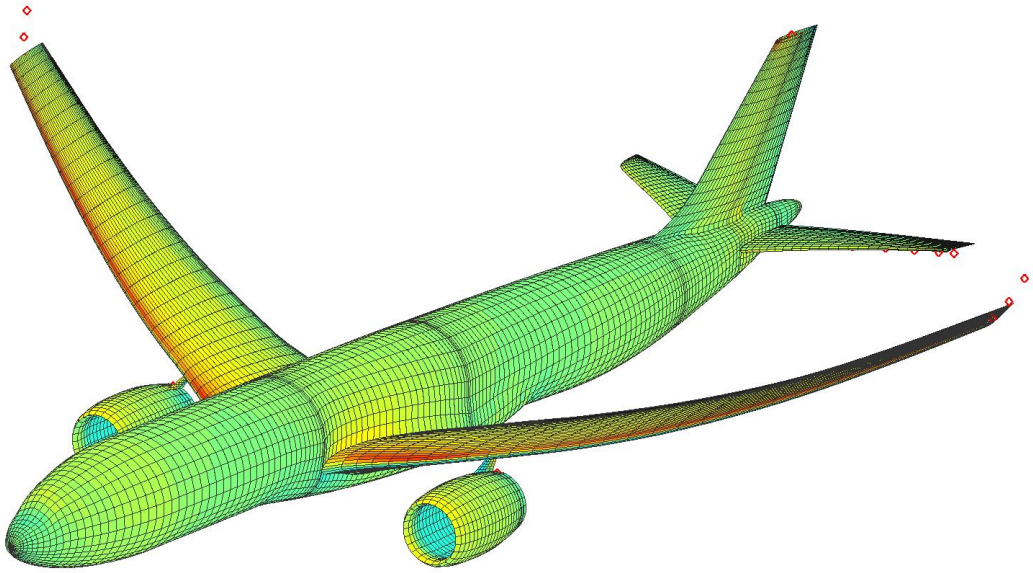

Figure 8: pressure distribution due to a 2.5 g pull-up manoeuvre using an AIC based 3D panel method approach.

excellent. Due to the high load factor, a large deformation occurs which considerably alters

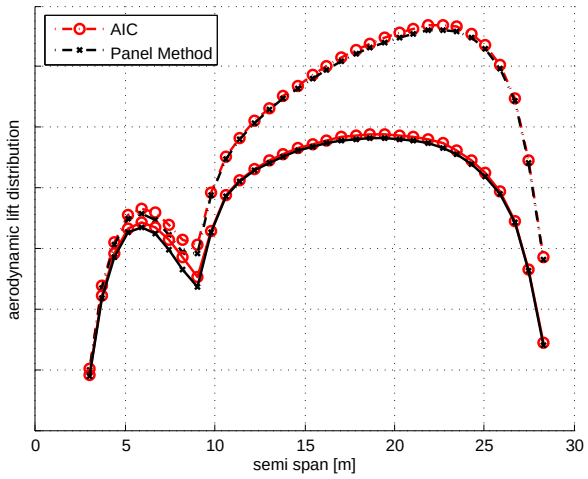

Figure 9: spanwise lift distribution, red for present AIC approach, black for Panel Method. Dashed lines are without flexible increment

the lift distribution compared to the rigid aircraft. The flexible twist at the tip nearly reaches 5°. Therefore, additionally the lift distribution without the flexible increment is depicted with dashed lines. It should be noted that this does not represent a trim of the rigid aircraft, but merely shows the flexible effects on the lift distribution. A rigidly trimmed aircraft would have a much lower angle of attack, such that the integrated lift of the wing is roughly the same as in the flexible case.

The second test case is a transient roll manoeuvre. An open loop model is used for the simulation, i.e. no flight control laws are implemented. The manoeuvre is starting from horizontal flight, then a step input to the pilot roll command deflects the ailerons

and initiates the roll. The target is a steady roll rate of about $15\,^{\circ}/s$. The maximum roll angle of roughly $\Phi = 60^{\circ}$ is reached after 4 seconds. Then the sign of the roll command is reversed. Since the simulation model does not contain flight control laws, a rudder deflection is applied to keep the angle of sideslip low. These aggressive inputs, albeit somewhat unrealistic, were chosen to excite the structural dynamics of the aircraft. The resulting trajectories of the simulation are shown in figure 10. For the comparison in reference [12], some effects were omitted that either could not be captured by the steady computations, such as the influence of the modal velocities in equation (17), or were unrealistic due to the deficiencies of the former, crude interpolation, such as control surface effectivities. In figure 11 the generalized aerodynamic forces for the first ten modes are depicted. Although not perfect, the results are in very good agreement. The excitation of the structural dynamics in particular of the antisymmetrical modes can clearly be seen.

4 SUMMARY AND CONCLUSION

Aerodynamic Influence Coefficients (AICs) from a 3D panel method were successfully used in the model integration for loads analysis simulations. Compared to co-simulation schemes, the AIC approach allows a direct formulation of the model equations as a system of nonlinear ordinary differential equations. The fact that the AIC matrices can be generalized to a small size, reduces the computational cost and allows for very fast simulations. The pressures and loads can then be recovered in a postprocessing step. The setup of the AIC matrices happens in a preprocessing step. The stored results can then be reused for different mass cases and manoeuvre load conditions. This allows for a quick determination of the loads envelope for aircraft design in a loop capable environment.

Previously unaccounted flight mechanical effects can be seamlessly incorporated in loads simulations using the AICs from a 3D panel method. Comparisons with CFD computations and a VLM implementation showed that the derivatives of rolling moment due to sideslip $C_{\mathcal{L}_\beta}$, rolling moment due to yaw rate $C_{\mathcal{L}_r}$, and yawing moment due to roll rate C_{N_p} are inherently present in formulation of the 3D panel method, while the classic VLM merely reproduces lift due to roll rate derivatives. These effects are essential to reproduce flight mechanical modes such as the dutch roll. They also play a major role in the flutter mechanism of T-tailed aircraft.

Since the AICs of a 3D panel method are dependent on the flight state, a more involved interpolation scheme is required. In the present paper a method to build a so called AIC-ROM, based on proper orthogonal decomposition is presented. The novelty in the present approach is that the POD is applied directly to AIC matrices rather than pressures. This limits the number of required parameters to set up the ROM to those, associated with the major nonlinearities like e.g. the angle of attack α and sideslip β. Other effects influencing the aerodynamic load distribution, like flexibility or rotation rates, are accounted for by the linear gradient information of the AICs. Comparisons between direct steady computations and evaluation of the AIC-ROM showed a very good correlation.

The use of AIC matrices of 3D panel have the potential to vastly improve the fidelity and accuracy of manoeuvre and gust loads simulations, as well as flutter calculations for T-tailed aircraft.

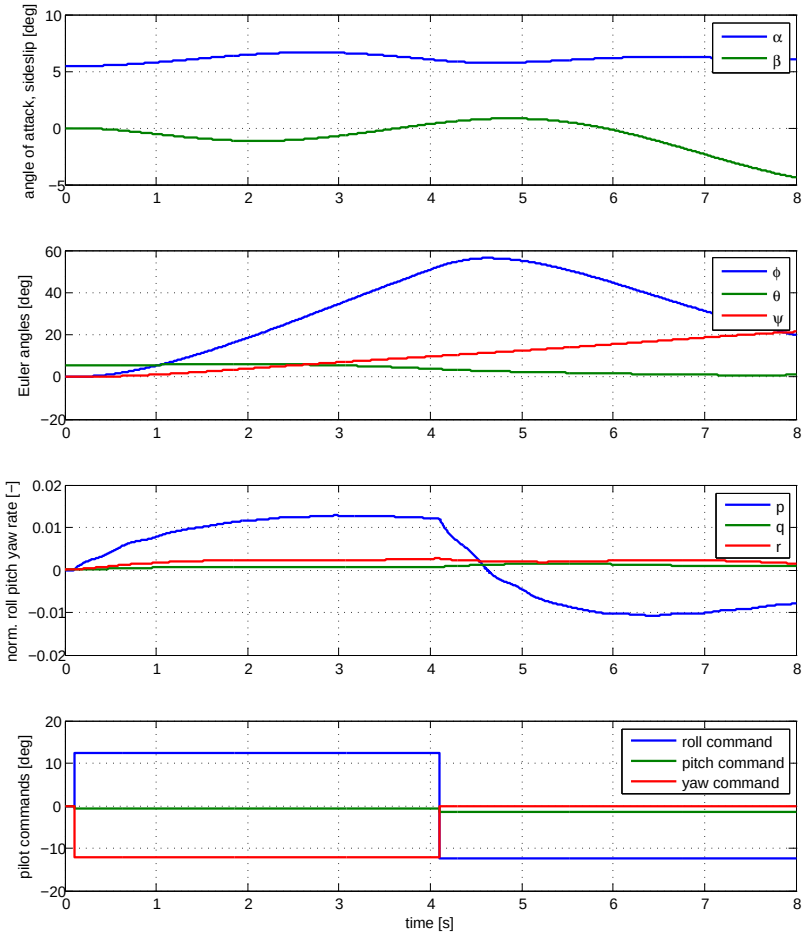

Figure 10: trajectories of the rolling manoeuvre

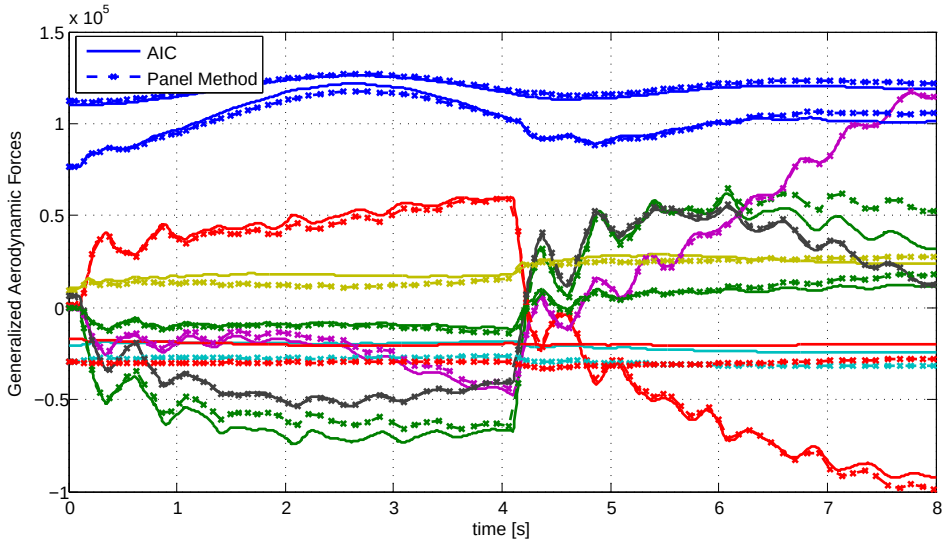

Figure 11: flexible generalized aerodynamic forces for AIC (solid) and panel method (dashed)

REFERENCES

[1] Hedman, S., "Vortex Lattice Method for Calculation of Quasi Steady State Loadings on Thin Elastic Wings," Tech. Rep. Report 105, Aeronautical Research Institute of Sweden, October 1965.

[2] Albano, E. and Rodden, W., "A Doublet-Lattice Method for Calculating Lift Distributions on Oscillating Surfaces in Subsonic Flows," *AIAA Journal*, Vol. 7, No. 2, 1969, pp. 279–285.

[3] W.P. Rodden, J. G. and Kalman, T., "New Developments and Applications of the Subsonic Doublet-Lattice Method for Nonplanar Configurations," *AGARD Symposium on unsteady aerodynamics for aeroelastic analyses of interfering surfaces*, No. AGARD-CP-80-71, AGARD, 1971.

[4] W.P. Rodden, P.F. Taylor and S.C. McIntosh Jr., "Further Refinement of the Subsonic Doublet-Lattice Method," *Journal of Aircraft*, Vol. 9, No. 10, 1998, pp. 693–702.

[5] Schütte, A., Einarsson, G., Raichle, A., Schöning, B., Orlt, M., J.Neumann, Arnold, J., Mönnich, W., and Forkert, T., "Numerical Simulation of Maneuvering Aircraft by Aerodynamic, Flight Mechanics and Structural Mechanics Coupling," *45th AIAA Aerospace Sciences Meeting and Exhibit, January 8-11, Reno, NV, USA*, No. AIAA 2007-1070, AIAA, January 2007.

[6] Ritter, M. and Dillinger, J., "Nonlinear Numerical Flight Dynamics for the Prediction of Maneuver Loads," *International Forum on Aeroelasticity and Structural Dynamics*, No. IFASD-2011-143, 2011.

[7] Christopher J. Sequeira, D. J. W. and Peraire, J., "Comparing Aerodynamic Models for Numerical Simulation of Dynamics and Control of Aircraft," *44th AIAA Aerospace Sciences Meeting and Exhibit*, No. AIAA 2006-1254, 2006.

[8] J. Katz and A. Plotkin, *Low Speed Aerodynamics: From Wing Theory to Panel Methods*, McGraw-Hill, 1991.

[9] Roger, K. L., "Airplane Math Modeling Methods for Active Control Design," *AGARD Structures and Materials Panel*, No. AGARD/CP-228, AGARD, April 1977, pp. 4–1 – 4–11.

[10] Kier, T. and Looye, G., "Unifying Manoeuvre and Gust Loads Analysis," *International Forum on Aeroelasticity and Structural Dynamics*, No. IFASD-2009-106, 2009.

[11] R. L. Bisplinghoff, H. Ashley, R. L. Halfman, *Aeroelasticity*, Dover Publications Inc., 1955.

[12] Kier, T. M., "Integrated Flexible Dynamic Maneuver Loads Models based on Aerodynamic Influence Coefficients of a 3D Panel Method," *56th AIAA/ASCE/AHS/ASC Structures, Structural Dynamics, and Materials Conference, 5-9 January 2015, Kissimmee, FL, USA*, No. AIAA 2015-0185, AIAA, 2015.

[13] Zimmermann, R. and Görtz, S., "Improved Extrapolation of Steady Turbulent Aerodynamics using a Non-Linear POD-based Reduced Order Model," *Aeronautical Journal*, Vol. 116, No. 1184, 2012, pp. 1079–1100.

[14] J. Hofstee, T. Kier, C. Cerulli, G. Looye, "A Variable, Fully Flexible Dynamic Response Tool for Special Investigations (VarLoads)," *International Forum on Aeroelasticity and Structural Dynamics*, 2003.

[15] T. Kier, G. Looye and J. Hofstee, "Development of Aircraft Flight Loads Analysis Models with Uncertainties for Pre-Design Studies," *International Forum on Aeroelasticity and Structural Dynamics*, June 2005.

[16] Kier, T. M., "Comparison of Unsteady Aerodynamic Modelling Methodologies with respect to Flight Loads Analysis," *AIAA Atmospheric Flight Mechanics Conference, 15-18 August, San Fancisco, CA, USA*, No. AIAA 2005-6027, AIAA, 2005.

[17] T. Kier, G. Looye, M. Scharpenberg, and M. Reijerkerk, "Process, Methods and Tools for Flexible Aircraft Flight Dynamics Model Integration," *International Forum on Aeroelasticity and Structural Dynamics*, No. IF-060, CEAS/AIAA, 2007.

[18] Kier, T., "An Integrated Loads Analysis Model including Unsteady Aerodynamic Effects for Position and Attitude dependent Gust Fields," *International Forum on Aeroelasticity and Structural Dynamics*, No. IFASD-2011-052, 2011.

[19] Kier, T., "An Integrated Loads Analysis Model for Wake Vortex Encounters," *International Forum on Aeroelasticity and Structural Dynamics*, No. IFASD-2013-30C, 2013.

[20] R. J. Guyan, "Reduction of stiffness and mass matrices," *Journal of Aircraft*, Vol. 3, No. 2, 1965, pp. 380.

[21] M. R. Waszak and D. K. Schmidt, "On the Flight Dynamics of Aeroelastic Vehicles," *AIAA Atmospheric Flight Mechanics Conference*, No. AIAA 86-2077, AIAA, 1986, pp. 120–133.

[22] M. R. Waszak and D. K. Schmidt, "Flight Dynamics of Aeroelastic Vehicles," *Journal of Aircraft*, Vol. 25, No. 6, 1988, pp. 563–571.

[23] M. R. Waszak, C. S. Buttrill and D. K. Schmidt, "Modeling and Model Simplification of Aeroelastic Vehicles: An Overview," Tech. Rep. NASA TM-107691, NASA LARC, 1992.

[24] Reschke, C., *Integrated Flight Loads Modelling and Analysis for Flexible Transport Aircraft*, Ph.D. thesis, Universität Stuttgart, 2006.

[25] Pistolesi, E., "Betrachtungen über die gegenseitige Beeinflussung von Tragflügelsystemen," *Gesammelte Vorträge der Hauptversammlung 1937 der Lilienthal Gesellschaft*, 1937.

[26] Harder, R. and Desmarais, R., "Interpolation Using Surface Splines," *Journal of Aircraft*, Vol. 9, No. 2, 1972, pp. 189–191.

[27] Rodden, W. P. and Johnson, E. H., *MSC.Nastran Aeroelastic Analysis User's Guide*, MSC, 1994.

[28] European Aviation Safety Agency, *Certification Specifications for Large Aeroplanes CS-25*, Vol. Subpart C - Structure, EASA, 2010.

[29] Theodorsen, T., "General Theory of Aerodynamic Instability and the Mechanism of Flutter," Tech. Rep. NACA Report 496, NACA, 1938.

[30] Flow Solutions Ltd., "NEWPAN," http://www.flowsol.co.uk/products/newpan/.

[31] Göthert, B., "Ebene und räumliche Strömung bei hohen Unterschallgeschwindigkeiten: Erweiterung der Prandtl'schen Regel," Tech. Rep. Bericht 127, Lilienthal Gessellschaft, 1940.

[32] Suciu, E., "MSC/NASTRAN Flutter Analyses of T-Tails including Horizontal Stabilizer Static Lift Effects and T-Tail Transonic Dip," *MSC/NASTRAN World User's Conference*, MSC, 1996.

[33] Murua, J., Martínez, P., Climent, H., van Zyl, L., and Palacios, R., "T-Tail Flutter: Potential-Flow Modelling And Experimental Validation," *International Forum on Aeroelasticity and Structural Dynamics*, No. IFASD-2013-22B, 2013.

[34] van Zyl, L., "Unsteady Panel Method for Complex Configurations Including Wake Modeling," *Journal of Aircraft*, Vol. 45, No. 1, 2008, pp. 276–285.

[35] van Zyl, L. and Mathews, E., "Aeroelastic Analysis of T-Tails Using an Enhanced Doublet Lattice Method," *Journal of Aircraft*, Vol. 48, No. 3, 2011, pp. 823–831.

[36] Malone, J. and Ruo, S., "LANN Wing Test Program: Acquisition and Application of Unsteady Transonic Data for Evaluation of Three-Dimensional Computational Methods," Tech. Rep. AFWAL-TR-83-3006, Wright Lab., Wright-Patterson AFB, 1983.